Applying Carrier Sense Multiple Access to Industrial IoT at Terahertz Frequencies

Applying Carrier Sense Multiple Access to Industrial IoT at Terahertz Frequencies

Sara Cavallero, Chiara Buratti, Alexey Tsarev, Giampaolo Cuozzo, Emil Khayrov, Yuliya Gaidamaka, Roberto Verdone

***Abstract*—This paper considers an Industrial Internet of Things (IIoT) scenario, where wireless devices embedded with sensors are deployed over an industrial machine, and transmit the measured data to a final Gateway (GW) using Terahertz (THz) frequencies. To mitigate the path loss of such high frequencies, the GW is equipped with multiple radiating elements, thereby generating highly directive beams, while sensors have just one single radiating element for miniaturization purposes. In this scenario, we study the applicability of a slotted Carrier Sense Multiple Access with Collision Avoidance (CSMA/CA) from a mathematical perspective. The analytical model is validated via comparison with simulations, and the impact of different simplifying assumptions in shown. We also demonstrate the effectiveness of the CSMA/CA when compared to ALOHA, and we prove that propagation delays cannot be neglected at THz frequencies.**

***Index Terms*—Industrial Internet of Things, Terahertz communications, CSMA/CA protocol, Throughput, Propagation delay.**

I. Introduction

The fourth industrial revolution, also known as Industry 4.0, is enriching the manufacturing world with the use of Information and Communications Technologies [1]–[3]. In particular, the Industrial Internet of Things (IIoT) is one of the key enablers of the Industry 4.0 paradigm, where sensors and actuators are inserted in the control loop of industry machines to enhance the efficiency and security of industrial processes [4]–[9].

In this paper, we consider an industrial scenario where wireless devices embedded with sensors (hereafter denoted as *tags* or *nodes*) are deployed over an automation machine to collect meaningful data for predictive maintenance or digital twins applications. Tags send the recorded data to a centralized control unit, denoted as Gateway (GW). From the wireless communication perspective, this scenario is extremely challenging: the number of tags, as well as the corresponding data-rates, produce network throughput that can be as large as tens of Gbit/s [10], [11], and tag miniaturization imposes another fundamental constraint. These requirements cannot be fulfilled by current wireless technologies [12]–[14], and this opens up new possibilities, such as using higher frequencies. The TeraHertz (THz) band, that is, the interval of frequencies from 0.1 to 10 THz, offers bandwidths of several GHz which provide ultra-high data rates, while tag miniaturization will benefit from the smaller wavelengths [15]–[19].

In our scenario, tags and GW communicate in the THz band using a slotted Carrier Sense Multiple Access with Collision Avoidance (CSMA/CA) at Medium Access Control (MAC)-layer [20], [21]. This MAC protocol mitigates some limitations of simpler protocols, e.g., ALOHA, by introducing the sensing phase at the device side, while avoiding the complexity of high-performing solutions like FTDMA [22]. We assume that the GW is equipped with multiple radiating elements, while tags have only one radiating element for miniaturization purposes. Hence, the GW can generate highly directive beams in a time-division fashion, that is, it periodically sweeps the entire machine volume to gather data from tags, whereas nodes produce an omnidirectional radiation pattern. However, this asymmetry introduces the hidden terminal problem, since tags cannot sense the transmissions of other nodes. Therefore, to limit collisions, tags send Request to Send (RTS) packets to notify the GW that they have data ready to be transmitted, and the GW replies with a Clear to Send (CTS) packet indicating the tag it is allowed to transmit its data. Nevertheless, at THz frequencies, propagation delays can be larger or in the same order of magnitude as packet transmission times, even at short distances. For instance, a 100-byte packet can be transmitted in 0.8 ns with a bit rate of 1 Tbit/s, while the propagation delay at a distance of 1 m is 3.3 ns. This may prevent a tag to receive the CTS sent by the GW if the sensing duration is not suitably set. In contrast to many works in literature [23], [24], our protocol accounts for the above mentioned aspect.

The contribution of this work is to study the applicability of CSMA/CA to the presented IIoT scenario from a mathematical perspective. A Semi-Markov chain is proposed, and the solution of the system of transcendental equations is presented [25]–[27]. The model is used to derive the packet success probability, the network throughput, and the average delay characterizing our intra-machine scenario, accounting for both, Physical (PHY) and MAC-layers aspects. The corresponding numerical evaluations are compared with simulation results, by also spotting the impact of some mathematical assumptions.

The paper is organised as follows. The next section presents the related works, while Section III describes the system model. Sections IV, V, and VI report the slotted CSMA/CA protocol, its analytical model, and the performance metrics, respectively. Numerical results are provided in Section VII, while conclusions are drawn in Section VIII.

S. Cavallero, C. Buratti, G. Cuozzo and R. Verdone are with the Department DEI, University of Bologna, and Wi-Lab, CNIT, Italy. Email: {s.cavallero, c.buratti, giampaolo.cuozzo, roberto.verdone}@unibo.it.

A. Tsarev is with Peoples' Friendship University of Russia (RUDN University), Moscow, Russia. Email: atsarev@sci.pfu.edu.ru

E. Khayrov is with Higher School of Economics, National Research University, Moscow, Russia. Email: ekhayrov@hse.ru

Y. Gaidamaka is both with Peoples' Friendship University of Russia (RUDN University) and Federal Research Center "Computer Science and Control" of the Russian Academy of Sciences, Moscow, Russia. Email: gaydamaka-yuv@rudn.ru

II. Related Works

A. MAC Protocols at THz frequencies

In the current literature, few works have addressed protocols aspects when considering high frequencies, such as millimiter Wave (mmWave) or THz. In particular, this section focuses on papers dealing with CSMA-based solutions for these frequencies, in agreement with the content of the paper.

A CSMA-based protocol is considered in [28], where directional antennas are used to mitigate the high path loss while introducing deafness problem. Authors propose a receiver-initiated handshake to allow the transmitter to understand the receiver antenna direction, as well as to guarantee the transmitter-receiver synchronization. In contrast, in this paper the GW performs a 3D sweeping to search for tags, therefore the deafness problem is not present because tags produce omnidirectional radiation patterns, and the GW is the unique device which generates highly directional beams.

Other works dealing with CSMA protocols assume nodes are equipped with multiple radios (e.g., [29]): a THz radio for data communication and a radio working at a lower frequency for neighbors discovery. This approach results in very large delays for the second phase. To overcome the latter limit we assume that a single radio is present. Other CSMA-based protocols working at mmWave also consider one radio but both transmitter and receiver generate directional beams ((see, e.g., [30]–[33]) or they operate in omnidirectional mode for nodes discovery, as well as sensing of the channel; while they move to directional antennas for the transmission phase (e.g., [34], [35]). However, all these works do not take propagation delays into account, which instead is a crucial aspect at THz frequencies from the MAC-layer perspective.

In conclusion, to the best of the Authors' knowledge, most contributes deal with the use of CSMA at mmWaves, and there is no work studying the applicability of CSMA to THz communications, considering all the peculiarities of such high frequencies in the protocol design and validation phase.

B. Modelling CSMA/CA Protocols

The analytical modelling of CSMA/CA protocols have been largely addressed since the seminal work by Bianchi, who proposed a two-dimensional Markov chain to characterize the back-off behavior of each single node, working in agreement with the IEEE 802.11 standard [23]. Since then, Bianchi's model has been widely used as a framework, and it has been modified for addressing different network conditions and variations of CSMA/CA schemes. In particular, [36] incorporates general back-off parameters; [37], [38] consider finite retransmission attempts, while others have considered imperfect channel conditions in [39], [40]. Additionally, a great effort was made to extend the model to unsaturated networks; for instance, in [41]–[43], it is assumed that each node has a one-packet buffer, and a new packet is generated with a given probability only after the successful transmission of the previous packet. In this paper, we use the latter approach. Finally, [44], [45] propose a more realistic assumption in terms of freezing back-off counters. Indeed, Bianchi's model assumes that each station immediately reactivates and decrements its counter during back-off, whereas the IEEE 802.11 standard specifies that a back-off counter is decremented only after the channel continues to remain idle for a predefined slot time. This behaviour is also captured by the model presented in this paper.

As far as the hidden terminal problem is concerned, most of the aforementioned works assume ideal channel conditions, thanks to the use of RTS/CTS control packets (see, e.g., [37], [38]). More realistic models are considered in [39], [46], [47], where the performance depends on the probability that nodes can hear each other. Conversely, in our paper, the nodes are always hidden from the others because their omnidirectional radiation patterns produce poor link budgets.

With reference to the propagation delays, most of the works consider either an average, or a maximum value (see, e.g., [23], [48]). Another approach is presented in [49], where the propagation delays are modelled as integer multiples of the time slot duration, and they are used to assess the probability that two nodes can hear each other. Differently from these works, we set the slot duration based on the maximum propagation delay, such that the sensing phase allows nodes to receive the CTS sent by the GW independently from its propagation delay, thereby mitigating the hidden terminal problem. Moreover, we exploit the statistics of the propagation delays when modelling the performance metrics, such as the collision probability.
In addition, many of the previous papers either do not specify the duplexing scheme, or they assume that the central control unit is full-duplex. In contrast, we consider the worst-case scenario of a half-duplex communication between the GW and tags.

To sum up, this paper introduces the following novelties with respect to the works in literature:

- *Hidden terminal problem*: working at such high frequencies, since the tags are immersed in metal parts and are only equipped with an antenna, their communication distance is very small, in the order of few centimetres. In this way, no tag can hear the others, so they are not aware of RTS transmissions over the channel and, as a consequence, collisions occur between RTS and CTS control packets. So, in this scenario, the exchange of RTS and CTS control messages does not solve the issue of hidden terminal problem and therefore it must be considered in the design of the mathematical model.
- *Impact of propagation delays*: We include propagation delays in the problem formulation and protocol design, and we model the collision probability as a function of the spatial distribution of tags in the volume.
- *Impact of the half-duplex nature of the GW*: the GW cannot receive the RTS while it is transmitting the CTS. Indeed, our choice to adopt an half-duplex GW, rather than full-duplex [50], goes in the direction of avoiding the issue of deploying self-interference cancellation techniques. Hence, the considered design is simpler, cheaper and considers the worst-case scenario.

Fig. 1. The reference automation machine has tags (T) uniformly distributed inside it, that sends the collected data in uplink to the GW. Tags have only one antenna, while the GW has several antenna elements. This IIoT scenario is modeled as a 3D sphere of radius R, with the GW in its center and the tags distributed inside it.

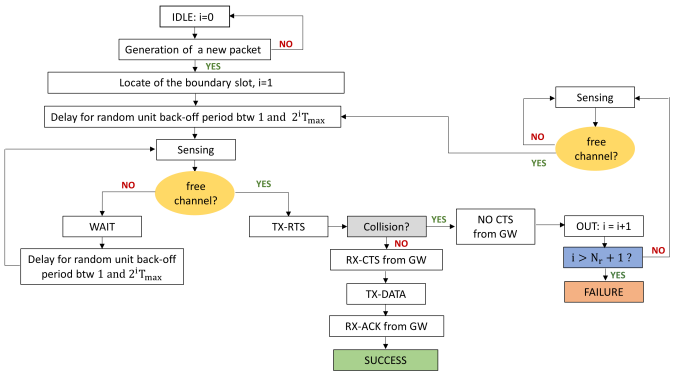

Fig. 2. State diagram of the slotted CSMA/CA protocol.

III. System Model

The reference scenario is an automation machine, with tags uniformly distributed inside it, collecting data in real time and sending it to the GW for the final processing. For the sake of simplicity, the reference automation machine is modeled as a 3D sphere of radius R and volume $V = \frac{4}{3}\pi R^3$, having the GW in its center (see Fig. 1). This choice derives from the assumption of a GW that radiates conical beams and their union shapes a sphere [51], [52].

Moreover, the GW is equipped with a number $N_{\rm a}$ of antenna elements, while tags have only one antenna. Therefore, the GW can generate an antenna beam with solid angle $\theta = 2\ arcsin(2/N_{\rm a})$ radiants. The resulting maximum antenna gain, G, can be assessed as [53]:

$$G = \frac{41000}{(\theta\ \frac{360}{2\pi})^2}\ . \tag{1}$$

The total number of beams in the sphere is $b = \frac{2}{(1-cos(\frac{\theta}{2}))}$, and each beam has a volume $V_\theta = \frac{2}{3}\pi R^3(1-cos(\theta/2))$.

We assume in each beam n_θ nodes are randomly and uniformly distributed, resulting in a total number of nodes in the sphere, $N = n_\theta\, b$. Once distributed, nodes stay still in positions known by the GW.

As far as the channel model is concerned, we consider the one presented in [54], [55]. The path-loss, $L_{\rm tot}$, for a traveling THz wave is given by:

$$L_{\rm tot}(d,f) = \left(\frac{4\pi f d}{c}\right)^2 e^{k(f)d}\, L_{\rm abs}\ , \tag{2}$$

where $(\frac{4\pi f d}{c})^2$ is the spreading loss, being d the total path length and f the frequency of the wave, while c stands for the speed of light in the vacuum. The term $e^{k(f)d}$ represents the molecular absorption attenuation, and $k(f)$ is the medium absorption coefficient, given by $k(f) = \sum_{i,g} k_{i,g}(f)$, where $k_{i,g}$ stands for the individual absorption coefficient for the isotopologue i of gas g [54]. It is worth mentioning that our analysis exploits the values of $k(f)$ that are used by the TeraSim simulator [56].

Finally, $L_{\rm abs}$ is the absorption loss due to the presence of metal in between transmitter and receiver (non-line-of-sight (NLOS) condition). In the following, we assume that the GW position allows to have GW-to-node links in line-of-sight (LOS) condition (i.e., $L_{\rm abs} = 0$ dB), while nodes are immersed into metal portions of the industrial machine, resulting in NLOS conditions for the node-to-node links.

IV. The slotted CSMA/CA MAC Protocol

Time is organized into frames, whose average duration will be denoted as $T_{\rm frame}$. Frames are divided into sub-frames, each dedicated to the exploration of one beam. Indeed, during each frame, the GW sweeps b beams, remaining in each of them for an average interval of time denoted as $T_{\rm b}$ (sub-frame duration). We assume the time needed to change the beam is negligible, as done in [57], [58]. Each sub-frame is divided into slots of duration $T_{\rm slot}$, and nodes can start a transmission only at the slot boundaries.

Figure 2 reports the state diagram of the slotted CSMA/CA protocol that nodes use at MAC-layer. In each sub-frame, the GW sends in broadcast a beacon packet to advise the tags the willingness of receiving their data packets. Each node will check its queue when receiving the beacon message. If the queue is empty, the node will wait for the next beacon. Otherwise, the tag performs back-off for a random number of time slots in the range $[1; 2^i T_{\rm max}]$, where $2^i T_{\rm max}$ is the maximum duration of the contention window, while i is an integer number which counts the number of transmissions attempts (i is set to 1 for the first transmission attempt). To limit collisions, each node performs sensing during the back-off period. If the tag senses a CTS transmission on the channel, it will delay the subsequent back-off (which is performed by keeping the same value of i), until the transmission occurring on the channel will finish. At the end of the back-off period, the node sends the RTS packet and it then goes in reception mode. The GW replies with a CTS in order to notify to all nodes that it is going to initiate a communication with a given device. When a tag receives the CTS, it will then transmit its data packet, in case the CTS was intended for it. Afterward, this selected node will receive the acknowldegment from the GW. Note that, in our scenario, collisions can still occur. More specifically, there are two possibilities:

1) *RTS-RTS collision*: It happens when an RTS arrives to the GW while it is receiving another RTS (see Figure 3). This type of collision takes place when two or more nodes are aligned in time. More in detail, this means that they have concluded their last back-off state at the same time, and they have also sensed a free channel.

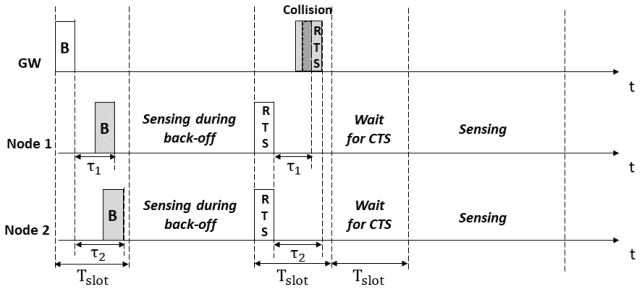

Fig. 3. Timing diagram of the collision between two RTS packets at GW-side.

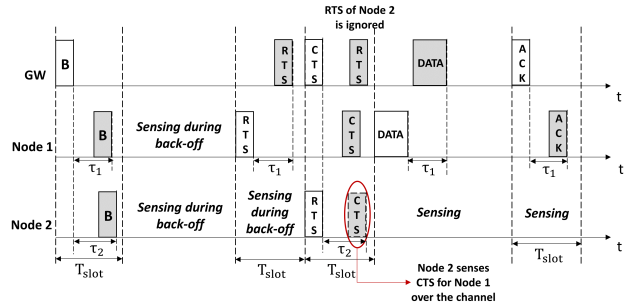

Fig. 4. Timing diagram of the collision between RTS and CTS packets at GW-side.

2) *RTS-CTS collision*: It happens when an RTS reaches the GW when it is transmitting the CTS packet. In Figure 4, Node 1 transmits its RTS message to the GW after having sensed a free channel during back-off, while Node 2 is still doing back-off. Due to the hidden terminal problem, Node 2 is not aware of RTS transmission from Node 1 and so it senses a free channel. In the next $T_{\rm slot}$, Node 2 transmits its RTS to the GW, but it is discarded because the GW is busy in transmitting the CTS to Node 1.

Remarkably, we assume that collisions are always harmful, that is, we consider an infinite capture threshold. Moreover, as we have already underlined, we assume that the GW is a half-duplex device, which means that the GW cannot simultaneously receive the RTS and transmit the CTS when the RTS-CTS collision occurs.

It is worth mentioning that, when a node receives a CTS which is intended to another tag, or it does not receive the CTS because of a RTS-RTS collision, it will again perform sensing until the channel is assessed to be free. Then, the node can start a new back-off stage, where i is increased by one. Sensing again the channel in this situation avoids subsequent collisions between RTS and data packets, as well as between RTS and acknowledgments. Notice that a node will not perform a new back-off stage if it has already made $(N_{\rm r}+1)$ attempts to transmit the RTS, where $N_{\rm r}$ is the maximum number of retransmissions. In this case, the corresponding data packet will be discarded.

A final remark refers to the time slot duration, which has been set by taking propagation delays into account, that is, to avoid that nodes do not receive the CTS because their sensing phase is not long enough. In this regard, we assume that beacon, RTS, CTS and acknowledgment packets have the same number of bytes L. Conversely, the data packet size will be denoted as $L_{\rm data}$, where it holds that $L_{\rm data} = n\,L$. Therefore, we set the slot duration equal to $T_{\rm slot} = L \cdot 8/R_{\rm b} + \tau_{\max}$, where $R_{\rm b}$ is the bit rate and $\tau_{\max} = \frac{R}{c}$ is the maximum propagation delay, which depends on the radius of the sphere R, and the speed of the light c. Note that the addition of $\tau_{\max}$ allows keeping synchronization and alignment among nodes, regardless of the specific propagation delay associated with each node.

V. Modelling the slotted CSMA/CA Protocol

This section presents the mathematical model which we have developed to derive the performance of the above described CSMA/CA protocol. The model captures the protocol states, together with the impact of the propagation delays. The performance will be evaluated in terms of success, collision, and channel-free probabilities, as well as network throughput and average delay. Let $X_{\rm MC}$ be the stochastic process representing the status of a given node. Tags remain in the different states for multiples of $T_{\rm slot}$. Since the status of a node in a given slot depends on its transmission history (e.g., the number of retransmissions), the stochastic process is non-Markovian. Nevertheless, we have still modelled $X_{\rm MC}$ with a Semi-Markov chain, thanks to the following three assumptions:

- **Assumption 1**: The collision probabilities for packets of different nodes are constant and independent each other, regardless of the number of retransmissions, that is, the number of collisions which have been experienced in the past;
- **Assumption 2**: The channel-free probabilities for different nodes are constant and independent of each other, regardless of the back-off stage, and the number of retransmissions;
- **Assumption 3**: The RTS-RTS collision event is independent from the RTS-CTS collision case.

Notice that Assumptions 1 and 2 are the same of both, the Bianchi's model, and its extensions [23]. The impact of these assumptions will be assessed in Section VII.

A. The Semi-Markov Chain Analysis

The stochastic process $X_{\rm MC}$ models the generic state where a node can be in a certain time slot. It is given by:

$$\begin{aligned} X_{\rm MC} = \{&IDLE, BO_1^{(1)}, ..., BO_1^{(N_{\rm r}+1)}, BO_{2T_{\max}}^{(1)}, ..., \\ &BO_{2T_{\max}}^{(N_{\rm r}+1)}, WAIT^{(1)}, ..., WAIT^{(N_{\rm r}+1)}, RTS^{(1)}, ..., \\ &RTS^{(N_{\rm r}+1)}, OUT_1^{(1)}, OUT_2^{(1)}, ..., OUT_1^{(N_{\rm r}+1)}, OUT_2^{(N_{\rm r}+1)}, \\ &RX_{\rm CTS}, WAIT_{\rm CTS}^{(1)}, ..., WAIT_{\rm CTS}^{(N_{\rm r}+1)}, DATA, ACK\}. \end{aligned} \tag{3}$$

In the following, we will describe in detail each single state appearing in eq. (3). In particular, each node remains in $IDLE$ state until it has no data packets to be transmitted to the GW. When a new data is generated, the node will move to the

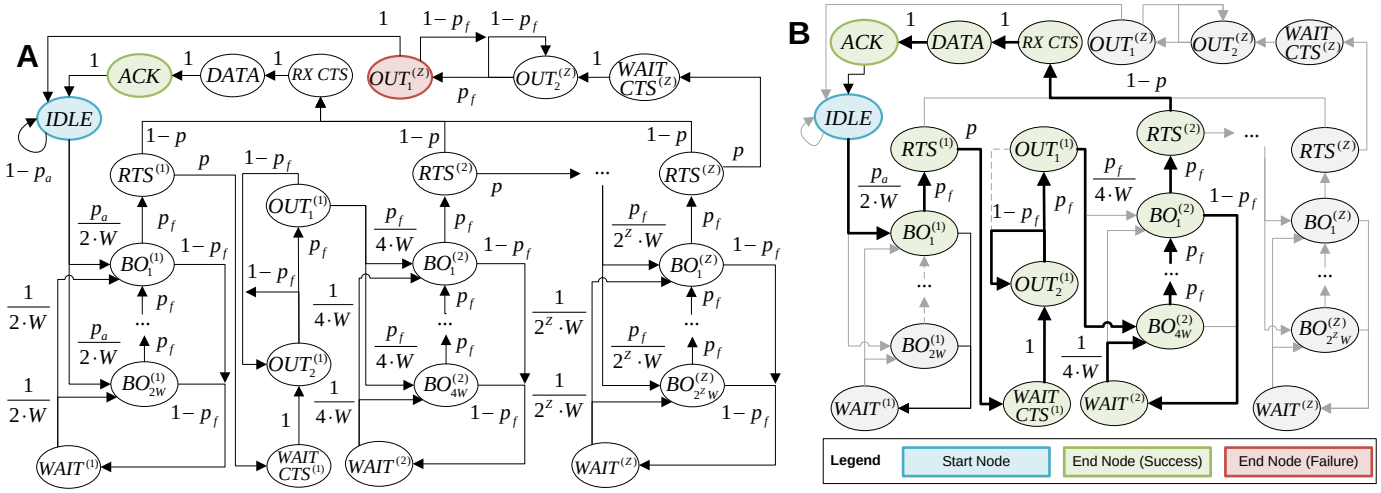

Fig. 5. Discrete Time Markov chain for CSMA/CA protocol. For the sake of compactness of the figure, we introduce $Z = N_{\rm r} + 1$ and $W = T_{\max}$. Figure A, shows the Discrete Time Markov chain underlying which are the states where the node starts and where the node ends in case of success or failure. Figure B, highlights via the green states the path followed by a node that is successful in sending data to the GW.

group of "BO" states, which models the different number of slots forming the back-off period. We recall that the back-off duration is an integer multiple of $T_{\rm slot}$, and this integer number is randomly and uniformly distributed between 1 and $2^i T_{\max}$, where $i = 1, .., (N_{\rm r} + 1)$ indicates the retransmission attempt. During back-off, a node goes into $WAIT^{(i)}$ state when it senses a CTS over the channel, and it remains in this state until the end of all the subsequent message exchanges (data and acknowledgment). If the channel is assessed as free for all back-off slots, the node enters the $RTS^{(i)}$ state, where it can perform the i-th transmission of the RTS. From this state, there are two possibilities. If the transmission of the RTS is successful, the node will move to state $RX_{\rm CTS}$, where it receives the corresponding CTS. Otherwise, the node will go in $WAIT^{(i)}_{\rm CTS}$, that is, it either receives the CTS which is not intended for it, or it does not receive any CTS.
From the $RX_{\rm CTS}$ state, the node will move into the $DATA$ state, where it transmits the data packet to the GW, assuming the data transmission lasts n slots. Afterward, the node will move to the ACK state, where it receives the acknowledgement from the GW, before entering again into $IDLE$ state.

From the $WAIT^{(i)}_{\rm CTS}$ state, the node goes through the set of "OUT" states, that is, $OUT_1^{(i)}$ and $OUT_2^{(i)}$. During both OUT states, a node performs sensing. If the channel is busy, the tag goes back to $OUT_2^{(i)}$ and the procedure restarts. Otherwise, if the channel is sensed free, the node again extracts an integer value between 1 and $2^{(i+1)}T_{\max}$ and it moves to the group of "BO" states. The aforementioned states form the Discrete Time (DT) Markov chain appearing in Figure 5. More specifically, we define:

- $p_{\rm a} \rightarrow$ probability that a node in $IDLE$ state has a packet ready to be transmitted;
- $p \rightarrow$ probability that a collision occur, i.e, an RTS-RTS or RTS-CTS collision event takes place;
- $p_{\rm f} \rightarrow$ probability that the channel is sensed as free.

By solving the DT Markov chain of Fig. 5, we obtain the following probability distributions, whose definitions are provided in table I:

TABLE I
STATIONARY PROBABILITIES OF DISCRETE TIME MARKOV CHAIN OVER $X_{\rm MC}$

Parameter	Definition
$\pi^{(\rm i)}_{\rm rts}$	prob. of being in RTS at attempt i
$\pi^{(\rm i)}_{\rm bo}$	prob. of being in BO at attempt i
$\pi^{(\rm i)}_{\rm wait}$	prob. of being in $WAIT$ at attempt i
$\pi^{(\rm i)}_{\rm wait_{cts}}$	prob. of being in $WAIT_{\rm cts}$ at attempt i
$\pi^{(\rm i)}_{\rm out_1}$	prob. of being in OUT_1 at attempt i
$\pi^{(\rm i)}_{\rm out_2}$	prob. of being in OUT_2 at attempt i
$\pi^{(\rm i)}_{\rm rx_{cts}}$	prob. of being in $RX_{\rm cts}$ at attempt i
$\pi^{(\rm i)}_{\rm ack}$	prob. of being in ACK at attempt i
$\pi^{(\rm i)}_{\rm data}$	prob. of being in $DATA$ at attempt i

$$\begin{cases} \pi^{(\rm i)}_{\rm rts} &= p^{i-1}\ p_{\rm a}\ \pi_{\rm idle}\,; \\ \pi^{(\rm i)}_{\rm bo} &= \frac{\pi_{\rm idle}\ \alpha}{(1-p_{\rm f})}\,; \\ \pi^{(\rm i)}_{\rm wait} &= \pi_{\rm idle}\ \alpha\,; \\ \pi^{(\rm i)}_{\rm wait_{cts}} &= p^{i}\ p_{\rm a}\ \pi_{\rm idle}\,; \\ \pi^{(\rm i)}_{\rm out_1} &= \frac{p^{i}\ p_{\rm a}}{p_{\rm f}}\ \pi_{\rm idle}\,; \\ \pi^{(\rm i)}_{\rm out_2} &= \frac{p^{i}\ p_{\rm a}}{p_{\rm f}^2}\ \pi_{\rm idle}\,; \\ \pi^{(\rm i)}_{\rm rx_{cts}} &= \pi^{(\rm i)}_{\rm ack} = \ \pi^{(\rm i)}_{\rm data} = (1-p)\ p^{i-1}\ p_{\rm a}\ \pi_{\rm idle}\,. \end{cases} \tag{4}$$

By imposing the total probability law:

$$\pi_{\rm idle} + \sum_{i=1}^{N_{\rm r}+1} \Big(\pi^{(i)}_{\rm rts} + \pi^{(i)}_{\rm bo} + \pi^{(i)}_{\rm wait} + \pi^{(i)}_{\rm wait_{cts}} + \pi^{(i)}_{\rm out_1} + \\ + \pi^{(i)}_{\rm out_2} + \pi^{(i)}_{\rm rx_{cts}} + \pi^{(i)}_{\rm data} + \pi^{(i)}_{\rm ack} \Big) = 1\,, \tag{5}$$

it is possible to derive the stationary distribution of the probabilities from global balance as follows:

$$\begin{cases} \pi_{\text{rts}} &= \sum_{i=1}^{N_\text{r}+1} \frac{p^{i-1}\, p_\text{a}}{D}\,; \\ \pi_{\text{bo}} &= \sum_{i=1}^{N_\text{r}+1} \frac{\alpha}{D\,(1-p_\text{f})}\,; \\ \pi_{\text{wait}} &= \sum_{i=1}^{N_\text{r}+1} \frac{\alpha}{D}\,; \\ \pi_{\text{wait}_\text{cts}} &= \sum_{i=1}^{N_\text{r}+1} \frac{p^i\, p_\text{a}}{D}\,; \\ \pi_{\text{out}_1} &= \sum_{i=1}^{N_\text{r}+1} \frac{p^i\, p_\text{a}}{D\, p_\text{f}}\,; \\ \pi_{\text{out}_2} &= \sum_{i=1}^{N_\text{r}+1} \frac{p^i\, p_\text{a}}{D\, p_\text{f}^2}\,; \\ \pi_{\text{rx}_\text{cts}} &= \pi_\text{ack} = \pi_\text{data} = \sum_{i=1}^{N_\text{r}+1} \frac{(1-p)\, p^{i-1}\, p_\text{a}}{D}\,; \\ \pi_{\text{idle}} &= \frac{1}{D}\,, \end{cases} \tag{6}$$

where:

$$\begin{cases} D &= 1 + \sum_{i=1}^{N_\text{r}+1} p^{i-1}\, p_\text{a}\, (\,1 + p + \frac{p}{p_\text{f}} + \frac{p}{p_\text{f}^2} \\ &\quad +(\frac{1}{1-p_\text{f}} + 1)\cdot \\ &\quad \cdot (\,\frac{(2^i\, T_\text{max}\,(\,1-p_\text{f}) - p_\text{f} + p_\text{f}^{2^i\, T_\text{max}+1})}{(p_\text{f} - p_\text{f}^{2^i\, T_\text{max}+1})}\,)+ \\ &\quad + 3\,(1-p)\,)\,; \\ \alpha &= \frac{p^{i-1}\, p_\text{a}\, (2^i\, T_\text{max}\,(\,1-p_\text{f}) - p_\text{f} + p_\text{f}^{2^i\, T_\text{max}+1})}{(p_\text{f} - p_\text{f}^{2^i\, T_\text{max}+1})}\,. \end{cases} \tag{7}$$

We then obtain a Semi-Markov process by including a state holding time. In particular, the *holding time* of state i, denoted as H_i, is the amount of time that passes before making a state transition from *i* [59]. More specifically, a node spends $H_\text{i,j}$ holding time in state *i* before moving to the next state *j*. State holding times are independent of the next state transition, that is, $H_\text{i,j} = H_\text{i}$ [59]. Moreover, we denote the stationary probability of the Semi-Markov process as Π_i, and the latter depends on the stationary probability of the DT Markov chain, π_i. A plausible conjecture is that Π_i is proportional to the product $\pi_\text{i}\mathbb{E}[H_\text{i}]$. Hence, we can write $\Pi_\text{i} = \pi_\text{i}\mathbb{E}[H_\text{i}]$. Consequently, the general set of stationary probabilities can be written as in table II:

$$\begin{cases} \Pi_{\text{rts}} &= \sum_{i=1}^{N_r+1} \frac{p^{i-1}\, p_\text{a}\, T_\text{rts}}{T_\text{b}}\,; \\ \Pi_{\text{bo}} &= \sum_{i=1}^{N_r+1} \frac{\alpha\, T_\text{bo}}{T_\text{b}\,(1-p_\text{f})}\,; \\ \Pi_{\text{wait}} &= \sum_{i=1}^{N_r+1} \frac{\alpha\, T_\text{wait}}{T_\text{b}}\,; \\ \Pi_{\text{wait}_\text{cts}} &= \sum_{i=1}^{N_r+1} \frac{p^i\, p_\text{a}\, T_{\text{wait}_\text{cts}}}{T_\text{b}}\,; \\ \Pi_{\text{out}_1} &= \sum_{i=1}^{N_r+1} \frac{p^i\, p_\text{a} T_{\text{out}_1}}{T_\text{b}\, p_\text{f}}\,; \\ \Pi_{\text{out}_2} &= \sum_{i=1}^{N_r+1} \frac{p^i\, p_\text{a} T_{\text{out}_2}}{T_\text{b}\, p_\text{f}^2}\,; \\ \Pi_{\text{rx}_\text{cts}} &= \sum_{i=1}^{N_r+1} \frac{(1-p)\, p^{i-1}\, p_\text{a}\, T_{\text{rx}_\text{cts}}}{T_\text{b}}\,; \\ \Pi_{\text{data}} &= \sum_{i=1}^{N_r+1} \frac{(1-p)\, p^{i-1}\, p_\text{a}\, T_\text{data}}{T_\text{b}}\,; \\ \Pi_{\text{ack}} &= \sum_{i=1}^{N_r+1} \frac{(1-p)\, p^{i-1}\, p_\text{a}\, T_\text{ack}}{T_\text{b}}\,; \\ \Pi_{\text{idle}} &= \frac{T_\text{idle}}{T_\text{b}}\,, \end{cases} \tag{8}$$

where T_b is the average cycle time duration (sub-frame duration), and it is a function of the average delay ξ. The latter is defined as the average interval of time between the instant in which a data packet is ready in the queue of the node, and the instant when the GW-to-tag communication ends. Notice that the communication can be concluded either with success, or with failure. In the former case, the GW has correctly received the data packet. In the latter, the tag has tried to unsuccessfully access the channel for $N_r + 1$ times, and thus it will discard the data packet from the queue. The expression of T_b is then

TABLE II
STATIONARY PROBABILITIES OF SEMI-MARKOV PROCESS OVER X_MC

Parameter	Definition
Π_rts	stationary prob. of being in RTS
Π_bo	stationary prob. of being in BO
Π_wait	stationary prob. of being in $WAIT$
$\Pi_{\text{wait}_\text{cts}}$	stationary prob. of being in $WAIT_\text{cts}$
Π_{out_1}	stationary prob. of being in OUT_1
Π_{out_2}	stationary prob. of being in OUT_2
$\Pi_{\text{rx}_\text{cts}}$	stationary prob. of being in RX_cts
Π_ack	stationary prob. of being in ACK
Π_data	stationary prob. of being in $DATA$

as follows:

$$\begin{aligned} T_\text{b} &= T_\text{idle} + p_\text{a}\,\xi\, = \\ &= T_\text{idle} + p_\text{a} \sum_{i=1}^{N_r+1} p^{i-1}\,(\,T_\text{rts} + p\,T_{\text{wait}_\text{cts}} + \\ &+ \frac{p\,T_{\text{out}_1}}{p_\text{f}} + \frac{p\,T_{\text{out}_2}}{p_\text{f}^2} + (\,\frac{T_\text{bo}}{1-p_\text{f}} + T_\text{wait}\,)\cdot \\ &\cdot (\,\frac{(2^i\, T_\text{max}\,(\,1-p_\text{f}) - p_\text{f} + p_\text{f}^{2^i\, T_\text{max}+1})}{(p_\text{f} - p_\text{f}^{2^i\, T_\text{max}+1})}\,) + \\ &+ (1-p)\,(T_{\text{rx}_\text{cts}} + T_\text{ack} + T_\text{data}))\,. \end{aligned} \tag{9}$$

All that being said, the time spent in each state is $T_\text{rts} = T_{\text{rx}_\text{cts}} = T_{\text{wait}_\text{cts}} = T_\text{ack} = T_\text{idle} = T_\text{bo} = T_\text{slot}$, while $T_\text{data} = T_\text{wait} = n\,T_\text{slot}$. Additionally, we set $T_{\text{out}_1} = T_\text{ack}$, and $T_{\text{out}_2} = T_\text{data}$. These two latter choices allow keeping nodes in OUT states for the entire time needed for data packet transmission and acknowledgment reception, thereby mitigating the collisions.

B. Collision and Channel-Free Probabilities

The overall collision probability, p, is the joint probability that an RTS packet collides with one (or more) RTS packets, or with the CTS message. The probability of the former is denoted as p_C, whereas the probability of the latter is denoted as p_I. Therefore, it holds that:

$$\begin{aligned} p &= \mathbb{P}\{\text{collision with RTS} \cup \text{collision with CTS}\} \\ &= \mathbb{P}\{\text{collision with RTS}\} + \mathbb{P}\{\text{collision with CTS}\} \\ &- \mathbb{P}\{\text{collision with RTS} \cap \text{collision with CTS}\}\,, \end{aligned} \tag{10}$$

where $\mathbb{P}\{\}$ is the probability of the event $\{\}$. For the sake of mathematical tractability, we approximate the above equation by using Assumpt. 3, i.e, the two collision events are independent. Eq. (V-B) can be then written as:

$$p \simeq p_\text{C} + p_\text{I} - p_\text{C}\cdot p_\text{I}\,. \tag{11}$$

The impact of the above approximation is assessed in Section VII. As far as p_C is concerned, its expression embeds the impact of propagation delays. In particular, the RTS packet of a node is not successfully received by the GW in case the difference between the propagation delay of the reference node, and those of at least one of the interfering nodes, is lower than the RTS transmission time, T_rts. If, instead, all the above

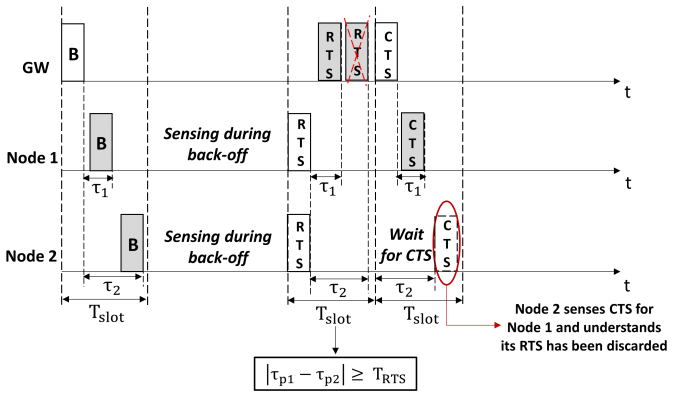

Fig. 6. Timing diagram of different RTS packets arriving at the GW when $|\tau_{\mathrm{p1}} - \tau_{\mathrm{p2}}| \geq T_{\mathrm{rts}}$. One RTS is successfully received and the other is discarded by the GW.

differences are larger or equal than T_{rts}, different RTS packets will be received by the GW within T_{slot}, but only one will be chosen by the GW (randomly) as winner of the channel, and the latter will be allowed to transmit its data packet by means of the CTS (see Fig. 6).
Therefore, p_{C} can be written as:

$$p_{\mathrm{C}} = \sum_{i=1}^{n_\theta - 1} \binom{n_\theta - 1}{i} \Pi_{\mathrm{bo_1}}^{i} (1 - \Pi_{\mathrm{bo_1}})^{n_\theta - 1 - i} \cdot \left[\sum_{j=1}^{i} \binom{i}{j} p_\tau^j (1-p_\tau)^{i-j} + \frac{i}{i+1}(1-p_\tau)^i \right],$$

where $\Pi_{\mathrm{bo_1}}$ is given by:

$$\Pi_{\mathrm{bo_1}} = \sum_{i=1}^{N_{\mathrm{r}}+1} \Pi_{\mathrm{bo_1}}^{(i)} = \sum_{i=1}^{N_{\mathrm{r}}+1} \frac{p^{i-1}\, p_{\mathrm{a}} T_{\mathrm{bo}}}{T_{\mathrm{b}}\, p_{\mathrm{f}}}. \tag{12}$$

The first term of (12) is the probability that at least another node, among the $n_\theta - 1$ present in the beam, is in the last back-off state BO_1, and it senses the channel as free, that is, it will transmit the RTS at the beginning of the subsequent time slot together with the reference node.
The second term, instead, accounts for the impact that propagation delays have on the collisions among RTS packets, as discussed at the beginning of this section. In particular, p_τ is the probability that the propagation delay of the reference node, denoted as $\tau_{\mathrm{p_0}}$, and of the interfering one, denoted as $\tau_{\mathrm{p_k}}$, is lower than the RTS transmission time, that is:

$$\begin{aligned} p_\tau &= \mathbb{P}\{|\tau_{\mathrm{p_0}} - \tau_{\mathrm{p_k}}| < T_{\mathrm{rts}}\} = 2\,\mathbb{P}\{\tau_{\mathrm{p_0}} - \tau_{\mathrm{p_k}} < T_{\mathrm{rts}}\} \\ &= 1 - 2\,\mathbb{P}\{d_0 - d_{\mathrm{k}} \geq T_{\mathrm{rts}}\, c\} \\ &= 1 - 2\int_{T_{\mathrm{rts}} c}^{R} \int_{0}^{d_0 - T_{\mathrm{rts}} c} \frac{3\, d_0^2}{R^3} \frac{3\, d_{\mathrm{k}}^2}{R^3} dd_0 dd_{\mathrm{k}}, \end{aligned}$$

where d_0 and d_{k} are the GW-to-node 0 and GW-to-node k distances, respectively. Note that p_τ is independent on the value of k, that is, the index of the interfering node. Moreover, it is worth noting that the product in eq. (12) is due to the independence of the two terms. Indeed, the collision probability at MAC-layer does not depend on the GW-to-node distance statistics, since we assume packets are lost if they collide, independently on the interference level.
As far as p_{I} is concerned, the RTS-CTS collision event occurs when a node transmits the RTS packet with success, and one or more other nodes transmit their RTS in the subsequent slot, thus colliding with the CTS transmission of the GW. Therefore, p_{I} accounts for the half-duplex nature of the GW and its expression is as follows:

$$p_{\mathrm{I}} = \left[(n_\theta - 1)\Pi_{\mathrm{rts}}\,(1 - \Pi_{\mathrm{rts}})^{n_\theta - 2}\right], \tag{13}$$

where there is a clear dependency on the stationary probability Π_{rts}.

Finally, we model the channel-free probability, p_{f}, as the probability that there are no CTS messages over the channel. Therefore, p_{f} is given by:

$$p_{\mathrm{f}} = 1 - \left[(n_\theta - 1)\Pi_{\mathrm{rts}}\,(1 - \Pi_{\mathrm{rts}})^{n_\theta - 2}\right]. \tag{14}$$

The accuracy of the presented mathematical formulation is estimated in Section VII, where we compare our model with simulation results.

VI. Performance Metrics

A. Packet Transmission Success Probability

The packet success probability, p_{s}, for node i at distance d_i from the GW, is given by:

$$p_{\mathrm{s}}(d_i, n_\theta) = p_{\mathrm{phy}}(d_i) \cdot p_{\mathrm{mac}}(n_\theta), \tag{15}$$

where the probability $p_{\mathrm{phy}}(d_i)$ accounts for PHY-layer aspects, whereas $p_{\mathrm{mac}}(n_\theta)$ accounts for MAC-layer aspects.
$p_{\mathrm{phy}}(d_i)$ is the success probability at PHY-layer, and it is computed as the product of the success probabilities of each independent packet (beacon, RTS, CTS and data) that node i has to transmit and receive from the GW. Let us define $p_{\mathrm{p}}(d, L)$ as the probability that the transmitted block of L bits at distance d is correctly decoded at the receiver side (node or GW).

Therefore, we have:

$$p_{\mathrm{phy}}(d_i) = p_{\mathrm{p}}(d_i, L)^3 \cdot p_{\mathrm{p}}(d_i, L_{\mathrm{data}}), \tag{16}$$

where we refer to Appendix A-B for the derivation of $p_{\mathrm{p}}(d, L)$.

$p_{\mathrm{mac}}(n_\theta)$, instead, is the success probability at MAC-layer, and it corresponds to the probability that an RTS packet, which is generated by a generic node in the network, is correctly received by the GW. We recall that, thanks to the considered RTS/CTS mechanism, a successful reception of the RTS at GW-side implies that the subsequent data packet transmission will be successful as well (i.e., the data packet cannot collide with other type of control or data plane messages). However, by leveraging on the definition of p and p_{a} (see Section V), it is possible to write the expression for the success probability at MAC-layer as follows:

$$p_{\mathrm{mac}} = \sum_{i=1}^{N_r+1} (1-p)\, p^{i-1}\, p_{\mathrm{a}}, \tag{17}$$

where we have neglected the dependency on n_θ to ease the notation.

B. Network Throughput

We define the network throughput as the number of information bits per unit of time which are correctly received by the GW. Then, if $\mathbf{d} = \{d_1, .., d_{\rm N}\}$ is the vector of GW-to-node distances, the network throughput can be written as:

$$S(\mathbf{d}) = \sum_{i=1}^{N} \frac{L_{\rm data}\, p_{\rm s}(d_i, n_\theta)}{T_{\rm frame}} = \\ = \sum_{i=1}^{N} \frac{L_{\rm data}\, p_{\rm phy}(d_i)\, p_{\rm mac}(n_\theta)}{b\, T_{\rm b}}\,, \tag{18}$$

where $L_{\rm data}$ is the number of bytes forming the data packet (it is assumed to be the same for all nodes). Furthermore, we recall that $T_{\rm frame}$ is the average time needed to gather data from all nodes, therefore to sweep the entire 3D sphere, while $T_{\rm b}$ is the average cycle time duration, where a cycle starts when a node in $IDLE$ state receives the beacon from the GW, and ends when the node goes back to $IDLE$ with success or failure.

Finally, we define the average network throughput, $\overline{S}$, averaged over the statistics of the distances, as follows:

$$\overline{S} = \frac{N\, L_{\rm data}\, \overline{p_{\rm phy}}\, p_{\rm mac}}{b\, T_{\rm b}} = \frac{n_\theta\, L_{\rm data}\, \overline{p_{\rm phy}}\, p_{\rm mac}}{T_{\rm b}}\,, \tag{19}$$

where we exploit the fact that $N = n_\theta\, b$, and $\overline{p_{\rm phy}}$ is given by:

$$\overline{p_{\rm phy}} = \int_{d_{\rm i}} p_{\rm phy}(d_{\rm i})\, \frac{3\, d_{\rm i}^2}{R^3}\, dd_{\rm i}\,. \tag{20}$$

C. Average Delay

We define the average delay, ξ, as the average interval of time between the instant in which a data packet is ready in the queue of the node, and the instant when the GW-to-tag communication ends. Specifically, the communication can finish with success (i.e, the data packet is correctly received by the GW), or with failure (i.e, the data packet has reached the maximum number of retransmissions $N_{\rm r}$).

VII. Numerical Results

In this section, we present and discuss some numerical results with the aim of i) showing the impact of the approximations introduced in the mathematical model, ii) comparing the slotted CSMA/CA protocol with ALOHA, and iii) underlying the impact of the propagation delays on the performance. Results are derived through both, numerical evaluations of our analytical model, and simulations. In particular, each simulation lasts $10^5\ T_{\rm slot}$, and the final performance metrics are obtained as the average of 500 simulations.

System parameters, if not otherwise specified, are reported in Table III. The number of antennas, $N_{\rm a}$, has been fixed in order to obtain $\gamma(d_{\rm i} = R) \geq \gamma_{\rm min}$, where the expression of $\gamma(d_{\rm i})$ can be found in Appendix A. Moreover, we assume that the minimum distance between nodes is 10 cm. This allows to have signal-to-noise ratios which are always lower than $\gamma_{\rm min}$ when setting $G = 1$, which is the gain characterizing the omnidirectional radiation pattern used by tags. Due to this configuration, tags cannot sense the RTS transmissions of other nodes, thereby introducing the hidden terminal problem in the considered scenario.

TABLE III
Parameter Settings

Parameter	Value	Parameter	Value
$N_{\rm r}$	3	$p_{\rm a}$	1
$T_{\rm max}$	12	M	5
f_c	1.025 THz[a]	Δf	10 GHz
B	50 GHz	T_0	290 K
$R_{\rm b}$	50 Gbit/s	$P_{\rm tx}$	7 mW
$\eta_{\rm t}$	1	$\eta_{\rm r}$	1
R	1 m	$\gamma_{\rm min}$	7 dB
$N_{\rm a}$	4	$L_{\rm abs}$	20 dB [61]
$L_{\rm rts}$	10 bytes	$L_{\rm data}$	{20, 100} bytes
$T_{\rm idle}$	1.6 ns	$T_{\rm bo}$	1.6 ns
$T_{\rm rts}$	1.6 ns	$T_{\rm out_1}$	1.6 ns
$T_{\rm ack}$	1.6 ns	$T_{\rm cts}$	1.6 ns
$T_{\rm wait}$	{3.2, 16} ns	$T_{\rm data} = T_{\rm out_2}$	{3.2, 16} ns

[a] According to Fig. 3 of [60], and by setting $f_{\rm c} = 1.025$ THz and $B = 50$ GHz, we consider a range of frequencies in between two peaks of the medium absorption coefficient.

A. Validating The Mathematical Model

Figure 7 shows the success, collision and channel-free probabilities at MAC layer for the considered CSMA/CA protocol, that is, $p_{\rm mac}$, p, and $p_{\rm f}$, as a function of the number of nodes per beam n_θ, and by comparing the mathematical model with simulations.
The data packet size is $L_{\rm data} = 20$ bytes. It is worth mentioning that propagation delays are not considered for this figure. As expected, $p_{\rm mac}$ and $p_{\rm f}$ decrease with n_θ, while the collision probability increases with the number of tags per beam.

As it can be seen, the comparison between the analytical model and simulations shows a good agreement, even though the gap slightly increases with n_θ. This non-perfect match is due to the combination of Assumptions 2 and 3 (see Sec. V), which produces an underestimation of the collision probability, resulting in an overestimation of the success probability at MAC layer. Assumption 1, instead, does not impact on the performance, as demonstrated in the next section.

B. Comparing ALOHA and CSMA-Based Protocols

In this section, we demonstrate the effectiveness of our CSMA/CA protocol when compared to ALOHA (the reader can refer to Appendix B for details about the ALOHA protocol).

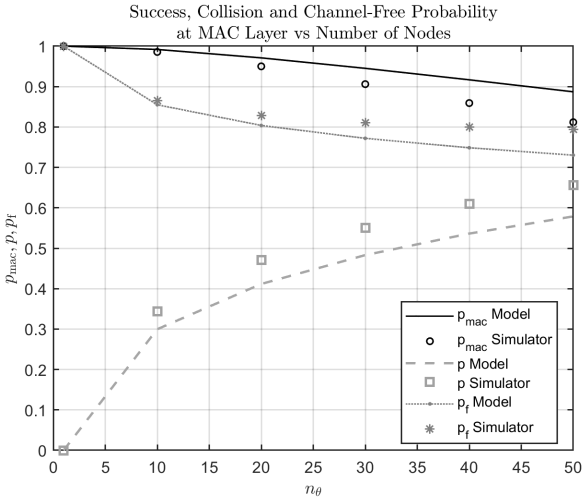

Fig. 7. Success, collision and channel-free probability of the considered CSMA/CA protocol as a function of n_θ, and by comparing our mathematical model with simulation results. We set $L_{\rm data} = 20$ bytes.

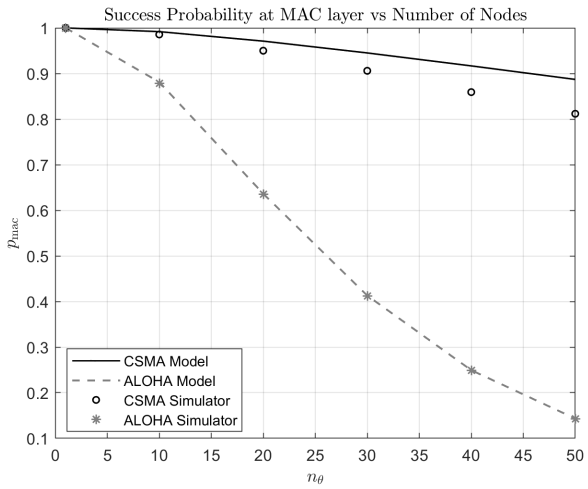

Fig. 8. Success probability at MAC level, $p_{\rm mac}$, as a function of n_θ, the protocol, i.e, CSMA/CA and ALOHA, and by comparing our mathematical model with simulations. We set $L_{\rm data} = 20$ bytes.

Figure 8 depicts the success probability at MAC layer, $p_{\rm mac}$, as a function of the number of nodes per beam n_θ[1], the protocol, that is, CSMA/CA and ALOHA, and by comparing our mathematical model with simulations. We still keep $L_{\rm data} = 20$ bytes for this plot. It can be seen that, for both protocols, $p_{\rm mac}$ decreases when n_θ increases, and the different slopes highlight that CSMA/CA is more resilient to collisions. Remarkably, ALOHA exhibits a perfect match between model and simulations in contrast to the considered CSMA/CA protocol. In fact, Assumption 1 is the unique approximation made for the mathematical modelling of ALOHA, thanks to the absence of sensing and control messages. This demonstrates that, for the considered CSMA/CA protocol, the mismatch between model and simulations is due to Assumption 2 and 3. Additionally, Figure 9 illustrates the average network throughput, $\overline{S}$, as a function of the number of tags in the sphere, N, the protocol, and by comparing our analytical model with simulations. In particular, we have $b = 14$, and we set $L_{\rm data} = 20$ bytes. As far as ALOHA is concerned, the average network throughput shows an optimum point. Indeed, by increasing N, there is a trade-off between the decay of $p_{\rm mac}$ due to more frequent collisions, and the rise of the average cycle time duration $T_{\rm b}$. This optimum point is right-hand shifted for the CSMA/CA protocol due to its better robustness towards collisions. The latter property is obtained by the use of RTS/CTS control packets, as well as the listen-before-talk paradigm.

C. The Impact of Propagation Delays

The impact of the propagation delays is assessed in this section. To this aim, we just rely on the numerical evaluations spreading out from the mathematical model of the CSMA/CA protocol.

[1]Having set $R = 1$ m and $N_{\rm a} = 4$, the beam volume results in $V_{\rm b} = 0.28$ m^3. Hence, for a density of 100 nodes/m^3, we have $n_\theta^{max} = 28$ nodes [62]; while for beyond-5G node densities, such as 200 nodes/m^3, we have $n_\theta^{max} \approx 50$ nodes, which is the maximum value considered in the x-axis of Figs. 7 and 8.

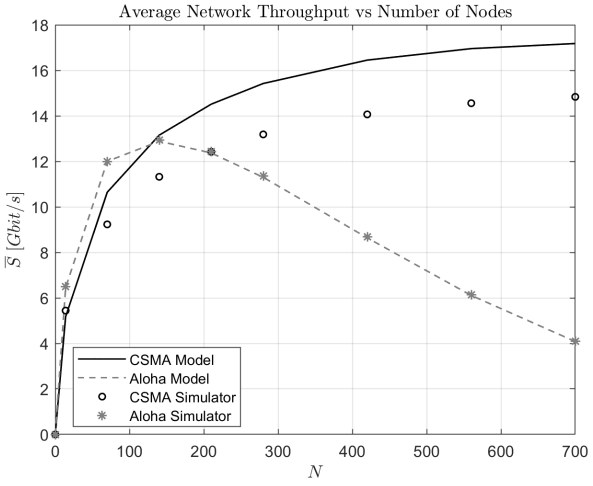

Fig. 9. Average network throughput, $\overline{S}$, as a function of N, the protocol, i.e, CSMA/CA and ALOHA, and by comparing our mathematical model with simulations. We set $L_{\rm data} = 20$ bytes.

Figure 10 shows the success probability at MAC layer, $p_{\rm mac}$, as a function of n_θ, the radius of the sphere R, the data packet size $L_{\rm data}$, and by also considering the benchmark case where propagation delays are neglected, that is, $\tau = 0$. Quite surprisingly, $p_{\rm mac}$ increases with R, meaning that longer propagation delays help in reducing collisions. Indeed, since transmissions are synchronised (i.e., all nodes start transmitting data at the same time), distributing nodes in a sufficiently wide space allows to increase the probability that packets reach the GW in different instants, thus limiting collisions. As underlined by eq. (13), if R increases, p_τ gets larger, resulting in lower collision probability, $p_{\rm C}$. This effect, however, is less pronounced when increasing the data packet size $L_{\rm data}$, since the impact of the propagation delay within the slot duration, $T_{\rm slot}$, gets lower. However, the figure proves our claim that the design of MAC protocols at THz frequencies should account for propagation delays, especially when the data packet size is low, since they affect the performance.

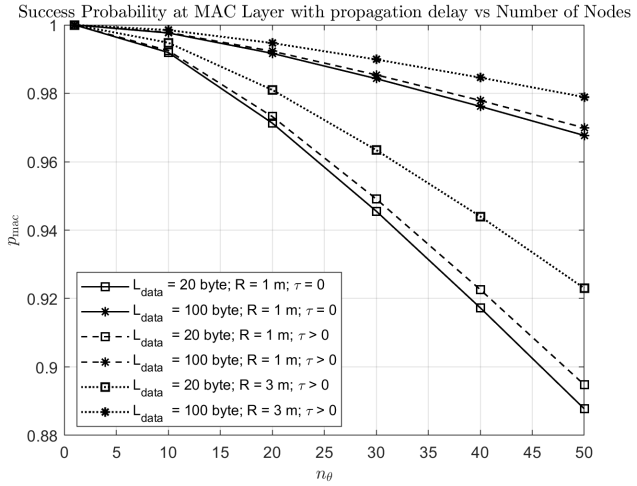

Fig. 10. Packet success probability at MAC layer, p_{mac}, as a function of n_θ, the radius of the sphere R, the data packet size L_{data}, and by also considering the benchmark case where propagation delays are neglected, that is, $\tau = 0$.

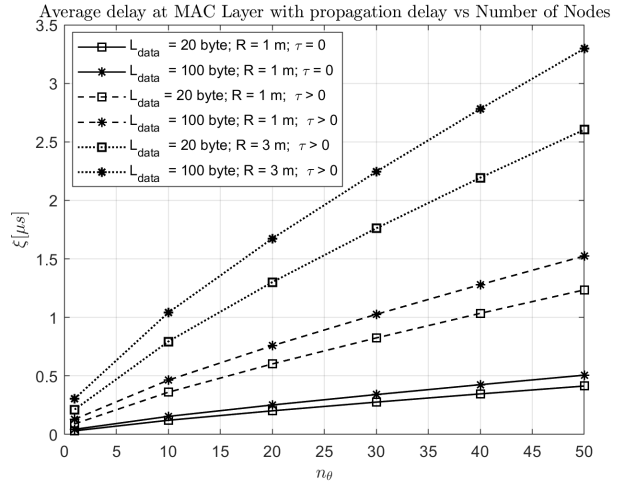

Fig. 11. Average delay, ξ, as a function of n_θ, the radius of the sphere R, the data packet size L_{data}, and by considering the cases where propagation delays are considered or neglected.

In Figure 11 we plot the average delay, ξ, as a function of n_θ, the radius of the sphere R, the data packet size L_{data}, and we again compare the case where propagation delays are considered or neglected. As expected, the average delay increases with n_θ and R, since longer propagation delays bring to higher values of T_{slot}.

Moreover, Figure 12 portrays the average network throughput, $\overline{S}$, as a function of n_θ, the radius of the sphere R, and the data packet size L_{data}. It is worth mentioning that we set $N_{\mathrm{a}} = 4$ for $R = 1$ m, and $N_{\mathrm{a}} = 21$ for $R = 3$ m. In this way, we have a fair comparison from the MAC-layer viewpoint, because $\overline{p_{\mathrm{phy}}}$ is fixed to 0.99 in both cases. As it can be seen from Fig. 12, the average network throughput decreases by increasing the propagation delay. This is due to the fact that the impact of the rise of ξ (i.e., T_{b} at the denominator of $\overline{S}$) when getting R larger is stronger than the improvement achieved in terms of p_{mac} (at the numerator of $\overline{S}$).

Finally, Table IV reports the comparison between model and

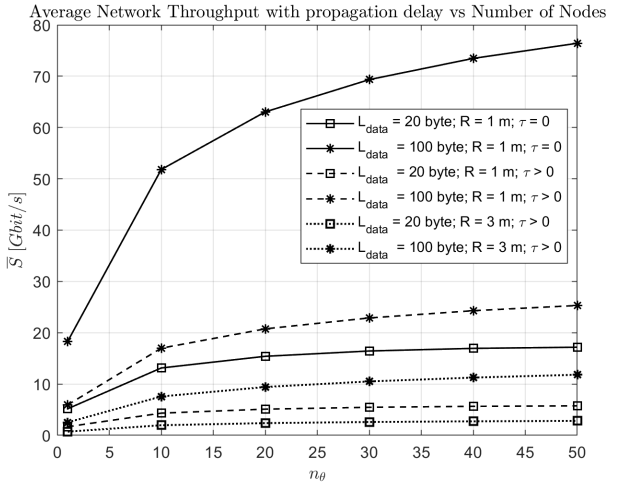

Fig. 12. Average network throughput, $\overline{S}$, as a function of n_θ, the radius of the sphere R, the data packet size L_{data}, and by considering the cases where propagation delays are considered or neglected.

TABLE IV
COMPARISON BETWEEN MODEL AND SIMULATION FOR p_{mac}, AND BY CONSIDERING PROPAGATION DELAYS.

n_θ	p_{mac} Model $R = 1$ m	p_{mac} Sim $R = 1$ m	p_{mac} Model $R = 3$ m	p_{mac} Sim $R = 3$ m
1	1	1	1	1
10	0.99	0.98	0.99	0.98
20	0.97	0.95	0.98	0.95
30	0.95	0.9	0.96	0.91
40	0.92	0.85	0.94	0.87
50	0.9	0.8	0.93	0.83

simulation for the success probability at MAC-layer, p_{mac}, as a function of the radius of the sphere R, and by taking propagation delays into account. Similar trends can be found for p, ξ, and $\overline{S}$.

VIII. CONCLUSIONS

In this paper, we study the applicability of CSMA/CA protocols to THz communications in an Industrial IoT scenario. To this aim, we have considered the peculiarities of the THz band, such as the introduction of the hidden terminal problem, and the impact of propagation delays. As far as the first effect is concerned, we deal with a slotted CSMA/CA which exploits RTS and CTS control packets to limit the collisions produced by the hidden terminal problem. Moreover, the protocol defines slots whose duration depends on the maximum propagation delay in the scenario, to ensure that all competing nodes receive the CTS. We then analytically model the slotted CSMA/CA via a Semi-Markov chain which accounts for all the aforementioned aspects. We compare the model with simulation results, and we carefully underline the impact of the different approximations introduced in the mathematical analysis. Results also show that propagation delays can help in reducing the collision probability, letting packets reach the GW at different time instants, but the

network throughput shrinks due to the increase of the slot duration.

APPENDIX A
PHYSICAL LAYER MODELLING

A. Signal-to-Noise Ratio

Molecular absorption does not only affect the properties of the channel in terms of attenuation; it also introduces noise [54]. In particular, the total noise temperature of the system, T_{noise}, is given by $T_{\text{noise}} = T_{\text{sys}} + T_{\text{mol}}$ where T_{sys} is the system electronic noise temperature, which for graphene-based electronic devices can be considered as negligible, due to the very low noise factors in nanomaterials [63]; T_{mol} is the equivalent noise temperature due to molecular absorption, given by $T_0\left(1-e^{-k(f)d}\right)$, where T_0 is the reference temperature. Finally, note that in our model we neglect sky noise, since at the frequency we are considering (1.025 THz) it is negligible w.r.t. molecular noise (see Fig. 2 in [64]).

The Signal-to-Noise Ratio (SNR) for the i-th node at distance d_{i} from the GW, on any of the sub-bands of width Δf, $\gamma(d_{\text{i}})$, is given by: $\gamma(d_{\text{i}}) = \frac{P_0(d_{\text{i}})}{P_{\text{n}}(d_{\text{i}})}$; the numerator $P_0(d_{\text{i}})$ is the received signal power:

$$P_0(d_{\text{i}}) = S_0\,\eta_{\text{t}}\,G_{\text{t}}\,\eta_{\text{r}}\,G_{\text{r}}\int_{\Delta f}\left(\frac{c}{4\pi f d_{\text{i}}}\right)^2\frac{e^{-k(f)d_{\text{i}}}}{L_{\text{abs}}}df\,, \quad (21)$$

where S_0 is the single-sided power spectral density of the transmitted signal (assumed to be flat in the bandwidth Δf and given by P_{tx}/B); G_{t} and G_{r} are the transmit and receive antenna gains and η_{t} and η_{r} are the transmit and receive antenna efficiencies. In our scenario, nodes have unitary antenna gain, while for the GW eq. (1) holds; therefore we have: $G_{\text{t}} = 1$ and $G_{\text{r}} = G$. $P_n(d_{\text{i}})$ is the noise power, given by:

$$P_n(d_{\text{i}}) = k_{\text{B}}\int_{\Delta f} T_{\text{noise}}\,df = k_{\text{B}}T_0\int_{\Delta f}(1-e^{-k(f)d_{\text{i}}})\,df\,, \quad (22)$$

where $k_{\text{B}} = 1.38\,10^{-23}$ J/K is the Boltzmann's constant.

This results in:

$$\gamma(d_{\text{i}}) = \frac{S_0\,G\,\eta_{\text{t}}\,\eta_{\text{r}}\int_{\Delta f}\left(\frac{c}{4\pi f d_{\text{i}}}\right)^2\frac{e^{-k(f)d_{\text{i}}}}{L_{\text{abs}}}df}{k_{\text{B}}T_0\int_{\Delta f}(1-e^{-k(f)d_{\text{i}}})\,df}\,. \quad (23)$$

B. Transmission Scheme and Modulation

We assume Frequency Division Multiplexing (FDM) is used: a control (or data) packet, made of L (or L_{data}) bytes, is fragmented over M sub-bands after serial-to-parallel conversion. In particular, the overall band of bandwidth B used by the system is divided into M sub-bands of width Δf, where the channel is assumed to be flat (i.e., the molecular absorption parameter $k(f)$ is constant) [54]. Each sub-band is centered around the carrier $f_{\text{k}} = f_{\text{c}} - \frac{B}{2} + (k-\frac{1}{2})\Delta f$, with $k = \{1,..,M\}$, being f_{c} the central frequency of the overall band.

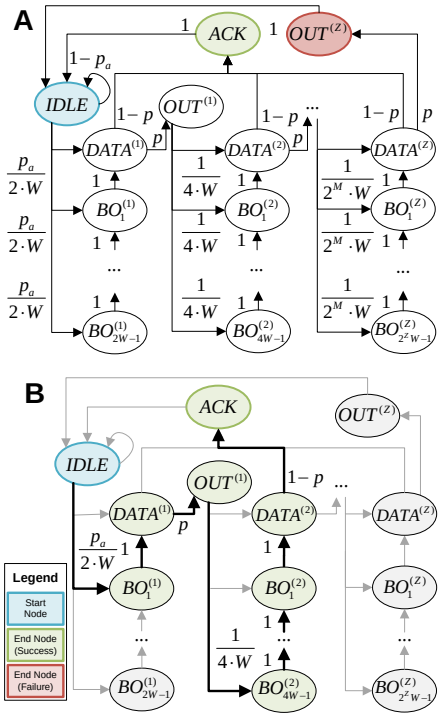

Fig. 13. Discrete Time Markov chain for ALOHA protocol. For the sake of compactness of the figure, we introduce $Z = N_{\text{r}}+1$ and $W = T_{\max}$. Figure A, shows the Discrete Time Markov chain underlying which are the states where the node starts and where the node ends in case of success or failure. Figure B, highlights via the green states the path followed by a node that is successful in sending data to the GW.

Since FDM is used, we need to compute the SNR at distance d_{i} with reference to the k-th sub-band of carrier f_{k}, which is given by:

$$\gamma(d_{\text{i}}, f_{\text{k}}) = \frac{S_0\,G\,\eta_{\text{t}}\,\eta_{\text{r}}\left(\frac{c}{4\pi f_{\text{k}} d_{\text{i}}}\right)^2\frac{e^{-k(f_{\text{k}})d_{\text{i}}}}{L_{\text{abs}}}}{k_{\text{B}}\,T_0\,(1-e^{-k(f_{\text{k}})d_{\text{i}}})}\,. \quad (24)$$

As for the modulation scheme for each branch of the multiplexer, without loss of generality we consider a Binary Phase Shift Keying (BPSK) scheme. Therefore, over the k-th sub-band, the Bit Error Rate, BER, is given by: $BER(d_{\text{i}}, f_{\text{k}}) = \frac{1}{2}\,erfc\sqrt{\gamma(d_{\text{i}}, f_{\text{k}})}$, where $erfc$ is the complementary error function.

Now, without loss of generality, we assume absence of Forward Error Correction (FEC) techniques; the entire block of bits is correctly received if they are all correct. Hence, $p_{\text{p}}(d, L)$ can be written as follows:

$$p_{\text{p}}(d, L) = \prod_{k=1}^{M}(1-BER(d, f_{\text{k}}))^{L/M}\,. \quad (25)$$

APPENDIX B
ALOHA PROTOCOL

In the slotted ALOHA protocol each node performs an initial random back-off, after which it transmits the data packet and waits for the acknowledgement from the GW if successful, otherwise it goes to OUT state and retries the transmission up to a maximum number of time, N_{r}. Fig. 13 represents the

Discrete Time Markov chain realized for ALOHA, similar to (5), where:

- p is the probability that a data packet transmitted on the channel collides with another data;
- $p_{\rm a}$ is the probability that a node in $IDLE$ has a packet ready to be transmitted in the queue.

Solving the Markov chain following the same procedure adopted for CSMA protocol, introducing the concept of Semi-Markov process and the holding time of each state multiple of $T_{\rm slot}$, we obtained the following stationary probabilities:

$$\begin{cases} \Pi_{\rm data} &= \sum_{i=1}^{N_{\rm r}+1} \frac{p^{i-1}\ p_{\rm a}\ T_{\rm data}}{T_{\rm b}}\ ; \\ \Pi_{\rm bo} &= \sum_{i=1}^{N_{\rm r}+1} \frac{\frac{1}{2}\ p^{i-1}\ p_{\rm a}\ (2^i\ T_{\rm max}-1)\ T_{\rm bo}}{T_{\rm b}}\ ; \\ \Pi_{\rm out} &= \sum_{i=1}^{N_{\rm r}+1} \frac{p^{i}\ p_{\rm a}\ T_{\rm out}}{T_{\rm b}}\ ; \\ \Pi_{\rm ack} &= \sum_{\rm i=1}^{N_{\rm r}+1} \frac{(1-p)\ p^{i-1}\ p_{\rm a}\ T_{\rm ack}}{T_{\rm b}}\ ; \\ \Pi_{\rm idle} &= \frac{T_{\rm idle}}{T_{\rm b}}\ , \end{cases} \tag{26}$$

where $T_{\rm b}$ is the average cycle time duration:

$$\begin{aligned} T_{\rm b} = T_{\rm idle}\ + p_{\rm a}\ \xi\ = \\ =\ T_{\rm idle}\ + p_{\rm a}\ \sum_{i=1}^{N_{\rm r}+1} p^{i-1}\ (\ T_{\rm data}\ +\ p\ T_{\rm out}\ + \\ +\ \frac{1}{2}\ (2^i\ T_{\rm max}-1)\ T_{\rm bo} +\ (1-p)\ T_{\rm ack})\ . \end{aligned} \tag{27}$$

The time spent in each state will be $T_{\rm idle} = T_{\rm ack} = T_{\rm bo} = T_{\rm out} = T_{\rm slot}$; then $T_{\rm data} = n\,T_{\rm slot}$.

A. Collision Probability

The collision probability p, is the probability that a data packet collides, which happens when at least another node, in addition to the reference one, transmits its packet within the vulnerable time period equal to $2\,T_{\rm data} - T_{\rm slot}$.

p can be modelled as:

$$p = 1 - (1 - p_{\rm data})^{(n_\theta - 1)}\ , \tag{28}$$

where $p_{\rm data}$ is the probability that a node is in DATA transmission within the vulnerability period:

$$p_{\rm data} = \sum_{i=1}^{N_{\rm r}+1} \frac{p^{i-1}\ p_{\rm a}\ (\ 2T_{\rm data} - T_{\rm slot}\ )}{T_{\rm b}}\ . \tag{29}$$

ACKNOWLEDGMENT

This work has been carried out within the COST CA20120 INTERACT Action framework.

REFERENCES

[1] P. Aceto and Pescapè, "A survey on information and communication technologies for industry 4.0: State-of-the-art, taxonomies, perspectives, and challenges." *IEEE Communications Surveys Tutorials*, vol. 21, no. 4, 2019.

[2] B. Bajic, A. Rikalovic, N. Suzic, and V. Piuri, "Industry 4.0 implementation challenges and opportunities: A managerial perspective," *IEEE Systems Journal*, vol. 15, no. 1, pp. 546–559, 2021.

[3] K. Zhou, T. Liu, and L. Zhou, "Industry 4.0: Towards future industrial opportunities and challenges," in *2015 12th International Conference on Fuzzy Systems and Knowledge Discovery (FSKD)*, 2015, pp. 2147–2152.

[4] J. Ding, M. Nemati, C. Ranaweera, and J. Choi, "Iot connectivity technologies and applications: A survey," *IEEE Access*, vol. 8, pp. 67 646–67 673, 2020.

[5] 5G-ACIA, "5G for Industrial Internet of Things (IIoT): Capabilities, Features, and Potential," *ZVEI*, November 2021.

[6] M. Wollschlaeger, T. Sauter, and J. Jasperneite, "The future of industrial communication: Automation networks in the era of the internet of things and industry 4.0," *IEEE industrial electronics magazine*, vol. 11, no. 1, pp. 17–27, March 2017.

[7] J. Cheng, W. Chen, F. Tao, and C.-L. Lin, "Industrial IoT in 5G environment towards smart manufacturing," *Journal of Industrial Information Integration*, vol. 10, pp. 10–19, June 2018.

[8] J. Lee, B. Bagheri, and H.-A. Kao, "A Cyber-Physical Systems architecture for Industry 4.0-based manufacturing systems," *Manufacturing Letters*, vol. 3, pp. 18 – 23, Jan. 2015.

[9] M. Younan, E. H. Houssein, M. Elhoseny, and A. A. Ali, "Challenges and recommended technologies for the industrial internet of things: A comprehensive review," *Measurement*, vol. 151, p. 107198, 2020.

[10] D. C. Nguyen, M. Ding, P. N. Pathirana, A. Seneviratne, J. Li, D. Niyato, O. Dobre, and H. V. Poor, "6g internet of things: A comprehensive survey," *IEEE Internet of Things Journal*, vol. 9, no. 1, pp. 359–383, 2022.

[11] P. Boronin, V. Petrov, D. Moltchanov, Y. Koucheryavy, and J. Jornet, "Capacity and throughput analysis of nanoscale machine communication through transparency windows in the terahertz band," *Nano Communication Networks*, vol. 5, 09 2014.

[12] S. Lin and L. Fu, "Throughput capacity of ieee 802.11 many-to/from-one bidirectional networks with physical-layer network coding," *IEEE Transactions on Wireless Communications*, vol. 15, no. 1, pp. 217–231, 2016.

[13] A. Waret, M. Kaneko, A. Guitton, and N. El Rachkidy, "Lora throughput analysis with imperfect spreading factor orthogonality," *IEEE Wireless Communications Letters*, vol. 8, no. 2, pp. 408–411, 2019.

[14] A. Dataesatu, P. Boonsrimuang, K. Mori, and P. Boonsrimuang, "Energy efficiency enhancement in 5g heterogeneous cellular networks using system throughput based sleep control scheme," in *2020 22nd International Conference on Advanced Communication Technology (ICACT)*, 2020, pp. 549–553.

[15] S. Ghafoor, N. Boujnah, M. H. Rehmani, and A. Davy, "MAC protocols for terahertz communication: A comprehensive survey," *Submitted to IEEE Comm. Surveys and Tut. Journal, arXiv:1904.11441*, 2019.

[16] S. Priebe and T. Kurner, "Stochastic modeling of thz indoor radio channels," *IEEE Trans. Wireless Commun.*, vol. 12, no. 9, p. 4445–4455, 2013.

[17] H. Elayan, O. Amin, R. M. Shubair, and M. Alouini, "Terahertz communication: The opportunities of wireless technology beyond 5g," in *2018 International Conference on Advanced Communication Technologies and Networking (CommNet)*, April 2018, pp. 1–5.

[18] F. Lemic, S. Abadal, W. Tavernier, P. Stroobant, D. Colle, E. Alarcón, J. Marquez-Barja, and J. Famaey, "Survey on terahertz nanocommunication and networking: A top-down perspective," *IEEE Journal on Selected Areas in Communications*, vol. 39, no. 6, pp. 1506–1543, 2021.

[19] Z. Chen, X. Ma, B. Zhang, Y. Zhang, Z. Niu, N. Kuang, W. Chen, L. Li, and S. Li, "A survey on terahertz communications," *China Communications*, vol. 16, no. 2, pp. 1–35, 2019.

[20] M. Youn, Y.-Y. Oh, J. Lee, and Y. Kim, "Ieee 802.15.4 based qos support slotted csma/ca mac for wireless sensor networks," in *2007 International Conference on Sensor Technologies and Applications (SENSORCOMM 2007)*, 2007, pp. 113–117.

[21] S. S, A. S. Adappa, K. D. Kumar, and A. Boyapati, "Implementation of unslotted and slotted csma/ca for 802.11 and 802.15.4 protocol," in *2019 Global Conference for Advancement in Technology (GCAT)*, 2019, pp. 1–7.

[22] A. B. Khalifa and R. Stanica, "Performance evaluation of channel access methods for dedicated iot networks," in *2019 Wireless Days (WD)*, 2019, pp. 1–6.

[23] G. Bianchi, "Performance analysis of the ieee 802.11 distributed coordination function," *IEEE Journal on Selected Areas in Communications*, vol. 18, no. 3, pp. 535–547, 2000.

[24] X. Zhang, C. Han, and X. Wang, "Dual-radio-assisted (dra) mac protocols for distributed terahertz networks," *IEEE Open Journal of Vehicular Technology*, vol. 2, pp. 111–124, 2021.

[25] G. Bianchi, "IEEE 802.11-saturation throughput analysis," *IEEE communications letters*, vol. 2, no. 12, pp. 318–320, 1998.

[26] G. Bianchi and I. Tinnirello, "Remarks on IEEE 802.11 DCF performance analysis," *IEEE communications letters*, vol. 9, no. 8, pp. 765–767, 2005.

[27] K. E. Samouylov, Y. V. Gaidamaka, I. A. Gudkova, E. R. Zaripova, and S. Y. Shorgin, "Baseline analytical model for machine-type communications over 3gpp rach in lte-advanced networks," in *Computer and Information Sciences*, T. Czachórski, E. Gelenbe, K. Grochla, and R. Lent, Eds. Cham: Springer International Publishing, 2016, pp. 203–213.

[28] Q. Xia, Z. Hossain, M. J. Medley, and J. M. Jornet, "A link-layer synchronization and medium access control protocol for terahertz-band communication networks," *IEEE Trans. on Mob. Comp.*, pp. 1–1, 2019.

[29] X. W. Yao and J. M. Jornet, "TAB-MAC: assisted beamforming mac protocol for terahertz communication networks," *Nano Communication Networks*, vol. 9, pp. 36–42, 2016.

[30] E. Shihab, L. Cai, and J. Pan, "A distributed asynchronous directional-to-directional mac protocol for wireless ad hoc networks," *IEEE Transactions on Vehicular Technology*, vol. 58, no. 9, pp. 5124–5134, 2009.

[31] H. Gossain, C. Cordeiro, D. Cavalcanti, and D. P. Agrawal, "The deafness problems and solutions in wireless ad hoc networks using directional antennas," in *IEEE Global Telecommunications Conference Workshops, 2004. GlobeCom Workshops 2004.*, 2004, pp. 108–113.

[32] M. X. Gong, D. Akhmetov, R. Want, and S. Mao, "Directional csma/ca protocol with spatial reuse for mmwave wireless networks," in *2010 IEEE Global Telecommunications Conference GLOBECOM 2010*, 2010, pp. 1–5.

[33] D. A. M. X. Gong, R. Stacey and S. Mao, "A directional csma/ca protocol for mmwave wireless pans," *Proc. IEEE Wireless Commun. Netw. Conf.*, pp. 1–6, Apr. 2010.

[34] A. Akhtar and S. C. Ergen, "Directional mac protocol for ieee 802.11ad based wireless local area networks," *Ad Hoc Networks*, vol. 69, pp. 49–64, 2018.

[35] R. Choudhury, X. Yang, R. Ramanathan, and N. Vaidya, "On designing mac protocols for wireless networks using directional antennas," *IEEE Transactions on Mobile Computing*, vol. 5, no. 5, pp. 477–491, 2006.

[36] A. Kumar, E. Altman, D. Miorandi, and M. Goyal, "New insights from a fixed-point analysis of single cell ieee 802.11 wlans," *IEEE/ACM Transactions on Networking*, vol. 15, no. 3, pp. 588–601, 2007.

[37] H. Wu, Y. Peng, K. Long, S. Cheng, and J. Ma, "Performance of reliable transport protocol over ieee 802.11 wireless lan: analysis and enhancement," in *Proceedings.Twenty-First Annual Joint Conference of the IEEE Computer and Communications Societies*, vol. 2, 2002, pp. 599–607 vol.2.

[38] J. Choi, J. Yoo, and C. kwon Kim, "A novel performance analysis model for an ieee 802.11 wireless lan," *IEEE Communications Letters*, vol. 10, no. 5, pp. 335–337, 2006.

[39] X. Li and Q.-A. Zeng, "Influence of bit error rate on the performance of ieee 802.11 mac protocol," in *2007 IEEE Wireless Communications and Networking Conference*, 2007, pp. 367–372.

[40] Y. Zheng, K. Lu, D. Wu, and Y. Fang, "Performance analysis of ieee 802.11 dcf in imperfect channels," *IEEE Transactions on Vehicular Technology*, vol. 55, no. 5, pp. 1648–1656, 2006.

[41] K. Duffy, D. Malone, and D. Leith, "Modeling the 802.11 distributed coordination function in non-saturated conditions," *IEEE Communications Letters*, vol. 9, no. 8, pp. 715–717, 2005.

[42] C. H. Foh, M. Zukerman, and J. W. Tantra, "A markovian framework for performance evaluation of ieee 802.11," *IEEE Transactions on Wireless Communications*, vol. 6, no. 4, pp. 1276–1265, 2007.

[43] D. Malone, K. Duffy, and D. Leith, "Modeling the 802.11 distributed coordination function in nonsaturated heterogeneous conditions," *IEEE/ACM Transactions on Networking*, vol. 15, no. 1, pp. 159–172, 2007.

[44] S. Sarkar, S. Misra, B. Bandyopadhyay, C. Chakraborty, and M. S. Obaidat, "Performance analysis of ieee 802.15.6 mac protocol under non-ideal channel conditions and saturated traffic regime," *IEEE Transactions on Computers*, vol. 64, no. 10, pp. 2912–2925, 2015.

[45] C. H. Foh and J. Tantra, "Comments on ieee 802.11 saturation throughput analysis with freezing of backoff counters," *IEEE Communications Letters*, vol. 9, no. 2, pp. 130–132, 2005.

[46] B. Jang and M. L. Sichitiu, "Ieee 802.11 saturation throughput analysis in the presence of hidden terminals," *IEEE/ACM Transactions on Networking*, vol. 20, no. 2, pp. 557–570, 2012.

[47] B. Nardelli and E. W. Knightly, "Closed-form throughput expressions for csma networks with collisions and hidden terminals," in *2012 Proceedings IEEE INFOCOM*, 2012, pp. 2309–2317.

[48] J. Simo Reigadas, A. Martinez-Fernandez, J. Ramos-Lopez, and J. Seoane-Pascual, "Modeling and optimizing ieee 802.11 dcf for long-distance links," *IEEE Transactions on Mobile Computing*, vol. 9, no. 6, pp. 881–896, 2010.

[49] A. Bhattacharya and A. Kumar, "Analytical modeling of ieee 802.11-type csma/ca networks with short term unfairness," *IEEE/ACM Transactions on Networking*, vol. 25, no. 6, pp. 3455–3472, 2017.

[50] D. Wrana, Y. Leiba, L. John, B. Schoch, A. Tessmann, and I. Kallfass, "Short-range full-duplex real-time wireless terahertz link for ieee802.15.3d applications," in *2022 IEEE Radio and Wireless Symposium (RWS)*, 2022, pp. 94–97.

[51] G. Ding, K. Chen, T. Jiang, B. Sima, J. Zhao, and Y. Feng, "Full control of conical beam carrying orbital angular momentum by reflective metasurface," *Opt. Express*, vol. 26, no. 16, pp. 20 990–21 002, Aug 2018. [Online]. Available: https://opg.optica.org/oe/abstract.cfm?URI=oe-26-16-20990

[52] W. He, L. Zhang, Y. He, and S.-W. Wong, "A wideband circularly polarized antenna with conical-beam radiation," in *2019 IEEE International Conference on RFID Technology and Applications (RFID-TA)*, 2019, pp. 444–447.

[53] Vijay Kumar Salvia, *Antenna and wave propagation*. Ed. Laxmi, 2007.

[54] J. M. Jornet and I. F. Akyildiz, "Channel modeling and capacity analysis for electromagnetic wireless nanonetworks in the terahertz band," *IEEE Transactions on Wireless Communications*, vol. 10, no. 10, pp. 3211–3221, 2011.

[55] C. Han, A. O. Bicen, and I. F. Akyildiz, "Multi-ray channel modeling and wideband characterization for wireless communications in the terahertz band," *IEEE Transactions on Wireless Communications*, vol. 14, no. 5, pp. 2402–2412, 2014.

[56] Z. Hossain, Q. Xia, and J. M. Jornet, "Terasim: An ns-3 extension to simulate terahertz-band communication networks," *Software Impacts*, vol. 1, p. 100004, 2019.

[57] F. Gao, B. Wang, C. Xing, J. An, and G. Y. Li, "Wideband beamforming for hybrid massive mimo terahertz communications," *IEEE Journal on Selected Areas in Communications*, vol. 39, no. 6, pp. 1725–1740, 2021.

[58] S. Xin, W. Ben-yuan, G. Li, and A. M. Liton, "Low delay and low overhead terahertz wireless personal area networks directional mac protocols," in *2021 6th International Conference on Intelligent Computing and Signal Processing (ICSP)*, 2021, pp. 687–691.

[59] Randolph Nelson, *Probability, Stochastic Processes, and Queueing Theory*, 1995.

[60] D. Slocum, E. Slingerland, R. Giles, and T. Goyette, "Atmospheric absorption of terahertz radiation and water vapor continuum effects," *Journal of Quantitative Spectroscopy and Radiative Transfer*, vol. 127, pp. 49–63, 09 2013.

[61] J. Fu, P. Juyal, and A. Zajić, "300 ghz channel characterization of chip-to-chip communication in metal enclosure," in *2019 13th European Conference on Antennas and Propagation (EuCAP)*, 2019, pp. 1–5.

[62] 5G-ACIA, "5G for Connected Industries and Automation," March 2019.

[63] A. N. Pal and A. Ghosh, "Ultralow noise field-effect transistor from multilayer graphene," *Applied Physics Letter*, vol. 95, no. 8, 2009.

[64] J. Kokkoniemi, J. Lehtomäki, and M. Juntti, "A discussion on molecular absorption noise in the terahertz band," *Nano Communication Networks*, vol. 8, pp. 35–45, 2016.

Sara Cavallero received the B.Sc in electronics and telecommunications engineering and the M.Sc with honors in telecommunications engineering from the University of Bologna, Bologna, Italy, in 2018 and 2021, respectively. She is currently pursuing the Ph.D. in electronics, telecommunications, and information technologies engineering (ETIT) at the University of Bologna.

Her research activity is focused on the design and modelling of MAC protocols for Industrial Internet of Things applications working at THz frequencies and the development of scheduling optimization algorithms of 5G NR networks to promote URLLC. She is also studying mathematical models based on Markov chains for the deployment of MAC protocols.

Chiara Buratti received the M.Sc. degree in telecommunications engineering from the University of Bologna, Bologna, Italy. She is an Assistant Professor with the University of Bologna. Since 2006, when she started her Ph.D., she has been involved in the research related to wireless networks for the Internet of Things, with particular reference to MAC and routing protocol design. She is currently a Principal Investigator of the COST Innovators' Grant IG15104, IMMUNet. She has been Main proponent of the Cost Action CA20120, INTERACT, and she is currently Vice-Chair and Grant Holder of the Action. She has been Chair of the EWG on IoT of the Cost Action IRACON, Dissemination Manager for the FP7 WiserBAN Project, and responsible of the EuWIn@Bologna laboratory, created within the FP7 NoE Newcom#. She has coauthored more than 90 research papers.

Alexey Tsarev received the B.Sc with honours in fundamental informatics and information technologies and the M.Sc with honours in fundamental informatics and information technologies from the RUDN University, Moscow, Russia, in 2016 and 2018, respectively. In 2021 he finished the Ph.D. studies in computer science at the RUDN University, his Ph.D. thesis defence is scheduled for 2022. His research activity is focused on the mathematical modelling and performance evaluation of 5G+ networks, which includes core networks, network virtualization, software-defined networking, MAC protocols and its applications. He is also involved in research and development activities at Netcracker Technology.

Giampaolo Cuozzo received from the University of Bologna the B.Sc with honors in electronics and telecommunications engineering in 2017, the M.Sc with honors in telecommunications engineering in 2019, and the Ph.D. degree in electronics, telecommunications, and information technologies engineering (ET-IT) in 2022.

He is currently Head of Research at the National Laboratory of Wireless Communications (WiLab) of CNIT (the National, Inter-University Consortium for Telecommunications). He is the author of 1 book, 1 invention, and 6 articles. His research activity is focused on the study, development, and validation of wireless networks for the Industrial Internet of Things, with a particular focus on signal processing techniques and MAC protocol design for THz-based systems, as well as scheduling optimization algorithms for 5G NR networks. His interests also include experimental activities that exploit current wireless technologies, like 5G, LoRa, Zigbee and NB-IoT.

Emil Khayrov received the B.Sc in applied mathematics and informatics and the M.Sc with honors in fundamental informatics and information technologies from the RUDN University, Moscow, Russia, in 2019 and 2021, respectively. Currently he is pursuing the Ph.D. in electronics, radio engineering and communication systems at the Higher School of Economics (HSE University). His research activity is focused at performance analysis in 5G+ networks, which includes MAC protocols for Industrial Internet of Things in THz, packet traffic analysis in both mmWave and THz, UAVs-based scenarios in mmWave networks and neural networks for image recognition.

Yuliya Gaidamaka received a PhD in 2001 and a Full Doctor of Sciences degree in 2017 in Mathematics from the Peoples' Friendship University of Russia (RUDN University). Since 2001, she has been an associate professor and currently a professor in the university's Applied Probability and Informatics Department. She is the author of more than 200 scientific and conference papers, co-author of three monographs on multiplicative solutions of finite Markov chains, matrix and analytical methods for performance analysis of wireless heterogeneous networks. Her current research focuses on performance analysis of 5G+ networks, queuing theory, mathematical modeling of communication networks including admission control, radio resource management using artificial intelligence. Her e-mail is gaydamaka-yuv@rudn.ru.

Roberto Verdone Roberto Verdone is full professor at the University of Bologna, since 2001. He is Director of WiLab, the Italian Laboratory of Wireless Communications of CNIT. He is also co-Director of the Joint Innovation Center on "Intelligent IoT for 6G" with Huawei. His main research interests are on the evolution from 5G to 6G, and the Internet of Things. He published 200 scientific papers and few books on various aspects of wireless communications.